Human Rett-derived neuronal progenitor cells in 3D graphene scaffold as an in vitro platform to study the effect of electrical stimulation on neuronal differentiation

Anh Tuan Nguyen [1,2,9], Sabrina Mattiassi [3.9], Manuela Loeblein [4,5], Eunice Chin [2], DongLiang Ma [2], Philippe Coquet [5], Virgile Viasnoff [1], Edwin Hang Tong Teo [4], Eyleen L. Goh [2,6], and Evelyn K.F. Yim [1,3,7,8]

[1] Mechanobiology Institute Singapore, National University of Singapore, T-Lab,#05-01, 5A Engineering Drive 1, 117411, Singapore

[2] Neuroscience Academic Clinical Programme, Duke-NUS Medical School, 20 college Road, 169856, Singapore

[3] Department of Chemical Engineering, University of Waterloo, 200 University Avenue West, Waterloo, Ontario, N2L 3G1, Canada,

[4] School of Electrical and Electronic Engineering, Nanyang Technological University, 50 Nanyang Avenue, 639798, Singapore,

[5] CNRS InternationalNTUThales Research Alliance (CINTRA) UMI 3288, Research Techno Plaza, 50 Nanyang Drive, 637553, Singapore

[6] National Neuroscience Institute, 11 Jalan Tan Tock Seng, 308433, Singapore

[7] Department of Biomedical Engineering, National University of Singapore, 4 Engineering Drive 3, Engineering Block 4,#04-08, 117583, Singapore

[8] Department of Surgery, Yong Loo Lin School of Medicine, National University of Singapore, NUHS Tower Block, 1E Kent Ridge Road, 119228, Singapore

[9] These authors have contributed to the work equally

E-mail: eyim@uwaterloo.ca

Abstract Studies of electrical stimulation therapies for the treatment of neurological disorders, such as deep brain stimulation, have almost exclusively been performed using animal-models. However, because animal-models can only approximate human brain disorders, these studies should be supplemented with an *in vitro* human cell-culture based model to substantiate the results of animal-based studies and further investigate therapeutic benefit in humans. This study presents a novel approach to analyse the effect of electrical stimulation on the neurogenesis of patient-induced pluripotent stem cell (iPSC) derived neural progenitor cell (NPC) lines, *in vitro* using a 3D graphene scaffold system**.** The iPSC-derived hNPCs used to demonstrate the system were collected from patients with Rett syndrome, a debilitating neurodevelopmental disorder. The graphene scaffold readily supported both the wild-type and Rett NPCs. Electrical stimulation parameters were optimized to accommodate both wild-type and Rett cells. Increased cell maturation and improvements in cell morphology of the Rett cells was observed after electrical stimulation. The results of the pilot study of electrical stimulation to enhance Rett NPCs neurogenesis were promising and support further investigation of the therapy. Overall, this system provides a valuable tool to study electrical stimulation as a potential therapy for neurological disorders using patient-specific cells.

Keywords:

Deep brain stimulation, Rett syndrome, Neurodevelopmental disease, Human induced pluripotent stem cells derived NPC, Neuronal maturation, Conductive 3D scaffold

1. Introduction

The use of electrical stimulation as a therapeutic treatment for patients with neurological degeneration or disease is well established. Deep brain stimulation (DBS) is an electrical stimulation therapy for the central nervous system in which electrodes are implanted into the brain and used to deliver electrical impulses. It is an effective but highly invasive procedure that has been used to successfully treat a variety of neurological disorders. DBS is currently accepted as effective for treating Parkinson's disease, essential tremor, dystonia, and is under consideration as a potential treatment of other neurological disorders such as psychiatric disorders, epilepsy and Alzheimer's disease (Kocabicak et al. 2015, Nardone et al. 2015, Thompson et al. 2014). Elucidation of the effect of DBS on neuron survival, development and differentiation could be used to better screen disease candidates for which DBS can be used therapeutically. A study model could also help to refine DBS therapy techniques allowing for optimization of therapeutic parameters such as improvement of target location and fine adjustment of electrical impulse parameters. Recently, experimental evidence indicated that DBS therapy in the hippocampus can have potentially therapeutic effects for childhood intellectual disability disorders.

One such disorder is Rett syndrome (RTT), a genetic post-natal neurodevelopmental disorder that is one of the leading causes of mental retardation in females (Hao et al. 2015, Lu et al. 2016). RTT patients develop seemingly normally up to six to 18 months of age, after which they start to display developmental stagnation. RTT patients experience general growth retardation, decelerated head growth leading to microcephaly, weight loss, and muscle hypotonia, in addition to loss of cognitive and motor skills (Chahrour and Zoghbi 2007). A major pathomorphological abnormality in the human RTT brain is the pronounced decrease in weight and volume. Individual neurons have small soma and they tend to pack more closely together. RTT neurons have diminished dendritic trees, leading to smaller observed cortical minicolumns, and fewer dendritic spines, with some neurons being spineless (Casanova et al. 2003, Belichenko et al. 1994). These morphological phenotypes indicate the formation of fewer neuronal connections in the RTT brain, leading to defects in neurotransmission. This has been corroborated by various RTT mouse models, whereby neurons

from the Mecp2-/y RTT mouse model were found to have reduced (by as much as 50%) synaptic outputs in their glutamatergic hippocampal neurons (Chao et al. 2007). Slice recordings from hippocampal and cortical brain slices of an Mecp2-null mouse model showed reduced long-term potentiation and impaired synaptic plasticity (Asaka et al. 2006). Encouragingly, DBS has been shown to be able rescue long-term hippocampal potentiation and increase hippocampal neurogenesis *in vivo* in the *Mecp2*$^{-/y}$ RTT mouse model. Further, DBS was able to rescue contextual fear memory, spatial learning and memory deficits in RTT animals (Hao et al. 2015). It is thus postulated DBS can be effective in the rescue of RTT by promoting neurogenesis.

Mouse models are widely used to screen electrical stimulation therapies for neurological disorders as they provide *in vivo* responses to treatment. While rodent studies may offer important precursory evidence, there is concern that the responses seen in the rodent models may not necessarily translate to humans. This is because the mouse models might not accurately reflect the physiological responses and neuronal development of human neuronal cells due to underlying neurological differences between humans and mice (Ananiev et al. 2011). Furthermore, the amount of throughput afforded by the model's cost and construct validity are greater in *in vitro* models than *in vivo* models. For instance, approximately 95% of classical Rett cases are due to mutations in the methyl-CpG-binding protein 2 (MECP2) gene, and the severity of RTT symptoms have been found to correlate to the location and type of mutations within the MECP2 gene (Amir et al. 1999, Wan et al. 1999, Amir et al. 2000, Bienvenu et al. 2000, Huppke et al. 2000, Lee et al. 2001). *In vitro* models, such as those that use induced pluripotent stem cells (iPSCs) reprogrammed from fibroblasts with RTT patient-specific MECP2 mutations, provide a ready platform that is more relevant to the disorder as they offer higher construct validity compared to loss-of-function cellular models. The models can be specified to any particular MECP2 mutation(s), which can have major ramifications on the study of disease mechanisms and screening of potential treatments given that variations in MECP2 mutations can affect the severity of symptoms. Additionally, it is easier and, in most cases, more cost-effective to scale up the number of conditions examined using *in vitro* models compared to *in vivo* models. Thus, an *in vitro* analysis using human cells will be useful to provide a platform to perform cellular studies

of an electrical stimulation therapy by high-throughput screening and supplement the results of *in vivo* analysis.

Using iPSC technology and a graphene scaffold-based method of *in vitro* modelling, the effect of electrical stimulation on the maturation of the RTT neuronal progenitor cells (NPCs) can be examined. This paper proposes the use of an electrically conductive cell-culturing system to test the effects of electrical stimulation on neurologically diseased human cells. The proposed scaffold is a three-dimensional (3D) graphene foam. Both two-dimensional (2D) and three-dimensional graphene scaffolds have previously been used with success to culture and electrically stimulate stem cells (Bouzid et al. 2016, Li et al. 2013). Graphene foams are mechanically stabile, flexible, easy to functionalize and have optical properties that make them suitable for bioimaging (Shin et al. 2016, Zhu et al. 2010). They also have easily tuneable surface properties and can be fabricated to mimic tissue-like structures, encouraging the correct alignment of neurons (Shin et al. 2016). Graphene in general is an excellent conductor and has significantly higher conductivity compared to graphene oxide (Gilje et al. 2007, Dreyer et al. 2010). Both 2D and 3D graphene structures have a suitable electrochemical window, however 3D graphene scaffolds have a higher double-layer capacitance compared to 2D graphene scaffold and a larger specific surface area (Li et al. 2013, Ameri et al. 2016). Three-dimensional graphene scaffolds also support neural stem cell adhesion, proliferation, and differentiation towards neurons (Loeblein et al. 2016, Ameri et al. 2016, Li et al. 2013).

While various studies have demonstrated the significance of studying neuronal cells in 3D systems (Zhang et al. 2016, Bosi et al. 2015, Soman et al. 2013) , the use of such systems as *in vitro* models of neuronal differentiation to study therapeutic techniques for treating neurodevelopment disorders, such as electrical stimulation, has not been extensively studied. Therefore, in this proof-of-concept study, we have developed a 3D-conductive scaffold system to study the effect of electrical stimulation on RTT patient-derived cells.

The encouraging *in vivo* results of electrical stimulation therapy for Rett syndrome shown by Hao et al. supports the concept that electrical stimulation can ameliorate the neurodevelopment defects

caused by Rett syndrome. We hypothesize that electrical stimulation will be able to enhance the maturation of neurons differentiated from iPSC-derived human NPCs (hNPCs) on a graphene scaffold. The conductive 3D-graphene scaffold culture system proposed in this paper addresses the research gap in the study and development of *in vitro* platforms for studying electrical stimulation therapy of neurological disorders, while simultaneously investigating the effect of electrical stimulation on the development of RTT NPCs cultured on conductive 3D scaffolds.

2. Materials and Methods

2.1. Three-dimensional graphene (3D-C) Fabrication and characterizations

Three-dimensional (3D) graphene (3D-C) was grown using thermal chemical vapor deposition (CVD). For this, a nickel (Ni) foam (Latech Scientific Supply Pte. Ltd.) was used as catalytic substrate. The Ni foam was placed in a split tube furnace and annealed for 5 minutes at 1000°C in ambient pressure, under argon (Ar) and hydrogen (H_2) flow. Subsequently the deposition process was started. In this process CH_4 was lead into the quartz tube with constant Ar and H_2 flow for 10 minutes to obtain complete coverage of graphene. After growth, the lid of the furnace was lifted for fast cooling. The obtained 3D-C/Ni sample was then dip-coated with poly(methyl methacrylate) (PMMA) to protect the carbon layers and immersed into hot HCl acid for at least 72 hours under constant refreshing of the etchant solution to completely remove the Ni. Afterwards the 3D-C was washed in DI-H_2O for another 72 hours under constant refreshing. Finally, to remove the PMMA coating, the samples were annealed at 700°C for one hour. Scaffolds with three different thicknesses, 0.5mm, 1 mm and 2 mm were produced. The density of the scaffold was determined by taking the entire volume of the Ni template foam as a block.

The electrical resistivity of the 3D-C (dimensions 1 cm x 1cm x 0.1 cm) was measured using the 4-point Van-der-Pauw method, which is a method applicable to structures of irregular geometry (Van der Pauw 1958). For this measurement, a current flow is induced along one edge of the sample, while measuring the voltage on its opposite side. This is repeated four times with alternating positioning of the current flow and voltage measurement.

Electron micrograph characterization of 3D-C was carried out using a scanning electron microscopy (SEM), JEOL JSM 5600LV at 15 keV. The samples were fixed in 3% glutaraldehyde at 4 ^{o}C overnight and then dehydrated with a series of ethanol solutions (30%, 50%, 70%, and 2x100%). Subsequently the samples were incubated in hexamethyldisilazane solution and allowed to air dry in a fume hood. Finally, the samples were gold coated and observed under the SEM. SEM images of the surface of 3D-C scaffold without cells and the cell-seeded scaffolds were captured.

2.2. Maintenance of hNPCs and Neural Differentiation

The generation and neural induction of iPSCs from Rett patient fibroblasts has been described previously (Chin et al. 2016). The hNPC lines and the isogenic control line without the MECP2 mutation (denoted as CTRL) were induced from iPSCs from one Rett patient with a 320 nucleotide deletion at nucleotide number 1155 (denoted as RTT). The Rett patient fibroblasts (GM11272) were purchased from Coriell Institute for Medical Research (New Jersey, USA). The neural progenitor cells used in this study were derived from induced pluripotent stem cells, which were reprogrammed from Rett patient-specific fibroblasts in the laboratory of the author EG; the induction and the preliminary characterizations were described in Chin et al. (Chin et al. 2016) as the same batches of cells were used in this study.

The hNPCs were maintained in the undifferentiated state using maintenance medium containing DMEM/F12 and neurobasal media (1:1 ratio, Gibco), 1% N2 supplement (Life Technologies), 2% B27 supplement (Life Technologies), 1X GlutaMAX^{TM} (Gibco), 1% penicillin/streptomycin (Gibco), 5 μg/mL bovine serum albumin (BSA), 3 μM CHIR99021 (Cellagentech), 2 μM SB431542, and 10 ng/mL human LIF (Millipore). Cells were cultured on Matrigel-coated plates with media replenished every alternate day. Accutase^{TM} (StemCell Technologies) was used as dissociated agent for cell passaging.

For neuronal differentiation, the maintenance medium was remove and replaced with differentiation media consisting of DMEM/F12 and neurobasal media (1:1 ratio), 1X N2 supplement, 1X B27 supplement, 1X GlutaMAX, 1X penicillin/streptomycin. Subsequently, half of the media was replaced every 2 days during maintenance.

Prior to cell seeding, 3D-C scaffolds were oxygen-plasma treated, UV-sterilized for 60 minutes in a biosafety cabinet (BSC), and subsequently coated with laminin (20 μg/mL at 4 ºC overnight. Then, the scaffolds were gently washed with 1X phosphate buffered solution (PBS) once and maintenance medium twice to remove the unbound laminin. Following an electrical resistance measurement to ensure the graphene was still well connected to the electrodes, hNPCs were seeded to the 3D-C scaffolds at a density of 2 million cells per scaffold (in a volume of 0.3 mL maintenance medium). Then, the cells were allowed to attach to the scaffold for 30 minutes before filling up the cell culture well with additional maintenance medium (a total of 3 mL medium in each well of a 6-well plate). hNPCs were left in maintenance medium for 24 hours after seeding to allow sufficient time to attach to and proliferate in the graphene scaffolds before applying electrical stimulation simultaneously with starting differentiation protocol. Initial characterization using RT-qPCR analysis of the hNPCs at day 0 to was done to examine expression of Nestin, SOX2, β-Tubulin III (TUJ1), glial fibrillary acidic protein (GFAP), microtubule-associated protein 2 (MAP2), synapsin I (Syn1), postsynaptic density protein 95 (PSD95), in both CTRL and RTT cells. This multipotency assay was done prior to cells seeding on the graphene scaffold.

2.3. Electrical Stimulation

At 24 hours from seeding, maintenance medium was removed and replenished with differentiation medium. Following medium changing, electrical stimulation of monophasic current was applied using a Keithley current source (Model 220). A unidirectional, square waveform with a frequency of 1 Hz and an amperage of 10 μA was applied for 30 min/day for the first 3 days of the differentiation protocol. As the amperage was controlled at 10 μA, the estimated voltage applied to each scaffold is ~20 μV. Characterization assays were carried out at different timepoints of 7, 11, and 21 days. Detailed information is described for each characterization assay in the following sections. The electrical stimulation procedure, apparatus and schematic are shown figure 1.

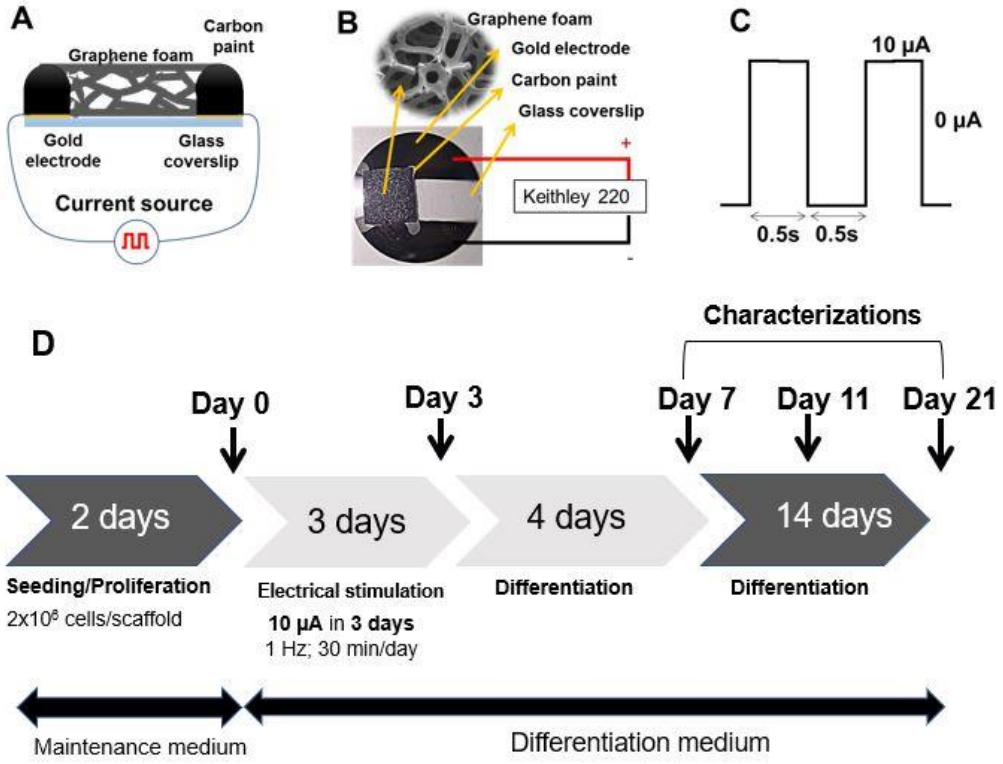

Figure 1*: (A) Schematic of electrical stimulation apparatus. (B) Picture of electrical stimulation apparatus. Scanning electron microscopy (SEM) image of the surface of scaffold is shown. (C) Uni-directional square waveform with a frequency of 1 Hz used for electrical stimulation. (D) Outline of experimental procedure. Cells were placed in differentiation medium on day 0 and then electrical stimulation began on day 3. Cells were stimulated for a total of 3 days. Cells were allowed to differentiation for a total of 14 days after stimulation. Characterization was done on day 7, day 11 and day 21 during the 14-day differentiation period.*

2.4. Cell Viability Assay

A Live/Dead® Viability/Cytotoxicity Kit (Molecular Probes) containing two reagents, Calcein AM and EthD-1, was used to assess the viability of hNPCs after the course of electrical stimulation according to the standard protocol provided by the manufacturer. A Leica epifluorescence microscope (Leica DMi8) was used to capture the images. Scanning electron microscopy (SEM) was employed to assess the morphologies of cells on the surface of the graphene scaffolds and cells cultured on a glass cover-slip.

2.5. Western Blot Analysis

Cells in the whole 3D-C scaffold were washed twice with ice-cold PBS 1X and lysed in cell lysis buffer. The scaffolds were broken into pieces and homogenized by re-suspending 5 times using a 23G needle

and 1 mL syringe. Cell lysates were centrifuged at maximum speed for 15 minutes at 4 ^{o}C and the supernatants were collected. Protein concentrations were measured using a Pierce^{TM} BCA Protein Assay Kit (Thermo Fisher Scientific). Samples were separated by using sodium dodecyl sulphate-polyacrylamide gel electrophoresis (SDS-PAGE) and then transferred to polyvinyl difluoride (PVDF) membranes. The membranes were blocked with 15 % BSA in Tris-buffer saline (TBS 1X) with 0.1% Tween 20 for 1 hour at room temperature, following by incubating with diluted primary antibodies at 4 ^{o}C overnight. The primary antibodies used were: rabbit anti-β-Tubulin III (TUJ1) (1:1000, Sigma-Aldrich), mouse anti-microtubule-associated protein 2 (MAP2) (1:500, Abcam), mouse anti-GAPDH (1:5000, Cell Signaling Technology). On the following day, the membranes were washed three times with TBS 1X with 0.1% Tween 20 and then incubated with the secondary antibodies (IgG-horseradish peroxidase conjugates, BioRad) for 1 hour at room temperature. ECL Western blotting substrate was used to detect immunoreactive bands (Clarity^{TM}, Bio-Rad). ImageJ was used for quantification of Western blot bands.

2.6. Real-time polymerase chain reaction (RT-qPCR) Analysis

For RT-qPCR experiment, total RNA was extracted from cells using the RNeasy Mini Kit (Qiagen). Complementary DNA (cDNA) was converted from total RNA using an iScript^{TM} cDNA synthesis kit (Bio-Rad). RT-qPCR measurements were carried out using SYBR green master mix (Bio-Rad) and a Bio-Rad CFX90 qPCR instrument. The qPCR analysis was calculated using the relative $\Delta\Delta C_t$ method, using GAPDH as the housekeeping gene (Kozera and Rapacz 2013, Chin et al. 2016). The primer sequences used can be found in table S1.

2.7. Immunofluorescence and Image Analysis

Cells were washed with PBS 1X and fixed with 4% paraformaldehyde for 15 minutes at room temperature. After permeabilized with 0.1 % Triton X-100 and blocked with 5% donkey serum in TBS 1X, samples were incubated overnight with primary antibodies at 4 ^{o}C. Primary antibodies used were: rabbit anti-TUJ1 (1:1000, Sigma-Aldrich), goat anti-DCX (1:500, Santa Cruz), mouse anti-MAP2 (1:500, Abcam). Next, the samples were washed thrice with TBS 1X, and then incubated with secondary antibodies (Alexa Fluor 488 or Alexa Fluor 546 conjugated donkey anti-rabbit, donkey-anti mouse, or donkey anti-goat secondary antibodies) for 1 hour at room temperature. After secondary antibody

incubation, samples were washed three times with TBS 1X and then stained with DAPI (1:2200, Invitrogen). Finally, the samples were washed thrice with PBS 1X before they were mounted on glass microscope slides using Fluoromount^{TM} (Sigma-Aldrich). Fluorescent images were acquired using a Zeiss LSM 710 confocal microscope.

Z-stack images were collected and divided into sub-stacks, each of which was 30 μm in depth. Cell Profiler was used to measure the percentage of cells positive for the neuronal markers of interest (TUJ1, MAP2 and DCX). The total number of cells was identified by counting the cells in the channel that contained DAPI stained nuclei. A threshold was applied to the channel with the neuronal marker of interest to reduce the amount of neurite extensions and this was then used as a mask. If the objects identified in the DAPI channel overlapped with those in the neuronal marker channel by at least 75% they were considered to the positive for the neuronal marker. The overlap criteria of 75% was set to prevent false positives occurring due to overlapping for neighbouring cells. The level of 75% was chosen as it was found that at this threshold, a minimal number of false positives and false negatives occurred. Verification was done by manually analysing select images and verifying whether or not cells were overlapping with neurite extensions. Soma size was measured using ImageJ by drawing regions of interest around soma and then measuring the area. The measured soma were then averaged to obtain average soma size.

2.8. Statistical Analysis

Statistical analysis of qPCR data was done using GraphPad Prism 7 software. Two-way t-tests and one-way ANOVA were used to compare the results from each treatment group and determine significance of results. In both tests the significance criteria was set to $p<0.05$. The number of replicas used for each calculation is stated in the figure legend.

3. Results

3.1. Characterization of the Graphene Scaffold

The graphene scaffolds closely resembled the structure of the Ni foam template (figure 2A) with a high porosity of 99.7% (250 – 400 μm in diameter of pore size) and high surface-volume ratio (~850 m^2/g) (Yavari et al. 2011). Since Ni is toxic to cells, it must be verified that it is completely removed

during etching. Etching for 72 hours under constant refreshing was shown to be sufficient to completely remove any supernatant Ni (with a residue of only ~6.7 ppb, (Loeblein et al. 2016), which is negligible compared to the level of metallic catalyser such as Sn or Zn found in polymers used for biomedical applications) (Albertsson and Varma 2003) . Using the Van-der-Pauw method outlined in Section 2.2, the 3D-C was measured to have a resistivity of $\rho = 1.7\ \Omega$cm (i.e. highly conducting).

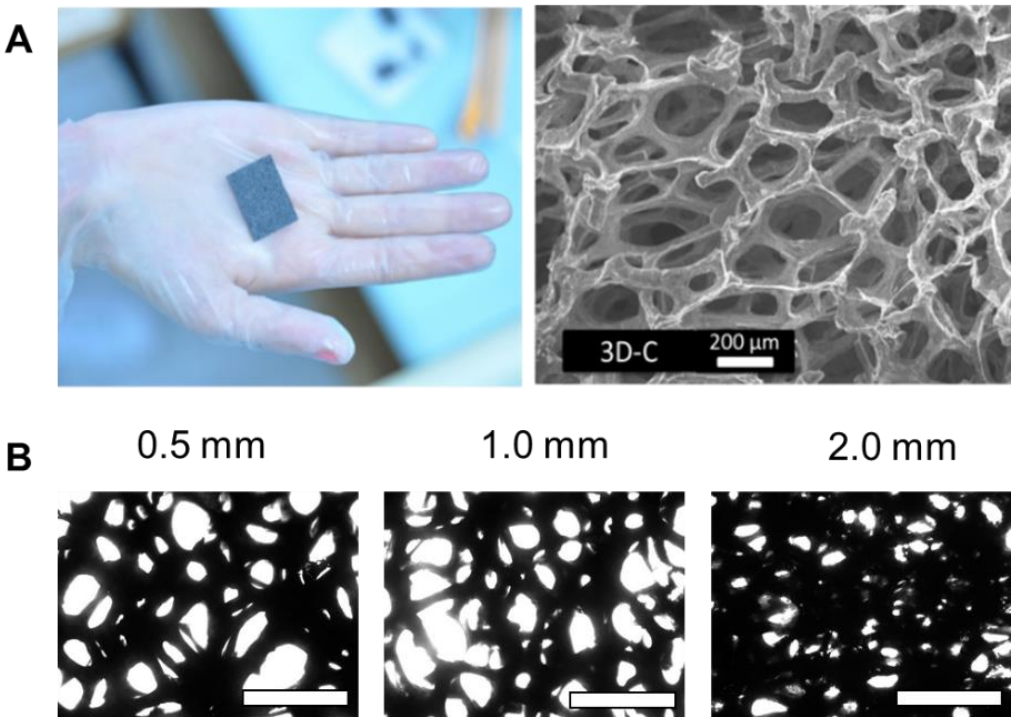

Figure 2: (A) Optical image and SEM image of the surface of a 3D graphene scaffold (3D-C). (B) Bright field images of the scaffolds with different thickness. The 1 mm thick scaffold was chosen in this study according to the feasibility in imaging the samples with light microscope (scale = 500 µm)

Scaffolds with three different thicknesses, 0.5mm, 1 mm and 2 mm, were produced and considered (figure 2B). The 0.5 mm thick scaffold was too thin and fragile for handling while the 2 mm one caused difficulty when imaging and characterizing samples with light microscopy. As shown in figure 2B, a significant portion of light was prevented from passing through the 2 mm thick scaffold. The 1 mm thick scaffold had neither of these problems and was deemed to be optimal for the study. The 1 mm thick scaffold was cut into 1 cm x 1 cm squares before cell seeding resulting in scaffolds with dimensions of 1 cm x 1 cm x 0.1 cm. Based on measurements of the whole Ni foam template, the density of the scaffold was determined to be 5 mg/cm^3. Using the measured density (5

mg/cm^3), porosity (high porosity (99.7%), volume (0.1 cm^3) and surface area-to-volume ratio (850 m^2/g), the total available surface area was estimated to be 12.75 cm^2.

3.2. Characterization of hNPC Lines

A RTT iPSC line and an isogenic control (CTRL) iPSC line were generated from a Rett patient using the nonintegrating episomal method and then induced into NPCs. Genotype analysis, analysis of embryonic germ layers, karyotyping analysis, immunostaining (not including day 0 characterization) and teratoma assays of the same batches of iPSCs and the derived-NPCs were performed and previously reported in Chin et al. (Chin et al. 2016). The genotype of the RTT donor patient had a frameshift mutation of MeCP2 due a 32-nucleotide deletion at nucleotide 1155. The resulting isogenic and RTT iPSCs lines were genotypically identical, but the isogenic line expressed wild-type MeCP2. Briefly, in the previous report, immunostaining and analysis of embryonic germ layers was done to confirm pluripotency of the cell lines. Clones from both cells lines stained positively for pluripotency markers (OCT4, Nanog, Tral-60 and SSEA4) and differentiation markers (AFP, SMA and DCX). All three embryonic germ layers contained derivatives with teratomas verifying *in vivo* differentiation. Additionally, in both cell lines no chromosomal defects were present and immunostaining for the X-inactivation marker histone 3 lysine 9 tri-methylation (H3K27me3) was positive. The iPSC cells lines were then differentiated into NPCs (Chin et al. 2016). To verify differentiation into NPCs Nestin and SOX2 were used as markers for immunostaining seven days post-induction. All cells in both cell lines were positive for both Nestin and SOX2 thus validating their status as NPCs. Procedures and protocols for the above assays are summarized in Section S1.1 and S1.2, and can also be found in Chin et al. (Chin et al. 2016).

To verify the cell characteristics of CTRL and RTT cells, NPC characterization using RT-qPCR at day 0, before seeding on the 3D-scaffold, was examined (figure S1). Both cells lines expressed the characteristic NPC marker genes Nestin and SOX2, with Nestin being expressed almost 3-times as much as SOX2. Expression of SOX2 was similar between the two cell lines however, Nestin expression was notably higher in the RTT NPCs. In both cell lines TUJ1 expression was

approximately the same as SOX2 expression. Both cell lines also had minimal expression of PSD95, and MAP2. Expression of Syn1 and GFAP was not observed in either cell line.

3.3. Optimization of Electrical Stimulation

Using CTRL cells, the parameters of electrical stimulation were optimized. The first parameter of electrical stimulation investigated was the amperage of the current. Direct currents in the micro and milli-ampere range were tested during optimization of electrical stimulation. Initially, 2 mA with a frequency of 1 Hz was tested and was found to be too harmful to the cells. Scanning electron microscopy (SEM) images showed that the unstimulated cells were able to attach and differentiate on the 3D-C scaffold but the cells that underwent 2 mA electrical stimulation showed apoptotic morphology (figures 3A and 3B). Moreover, TUJ1-positive neurites and neuronal networks were observed in immunofluorescent images of cells grown on the glass substrate and in the 3D-C scaffold without electrical stimulation, which indicate that cells were healthy, in contrast to the cells that were electrically stimulated with 2mA.

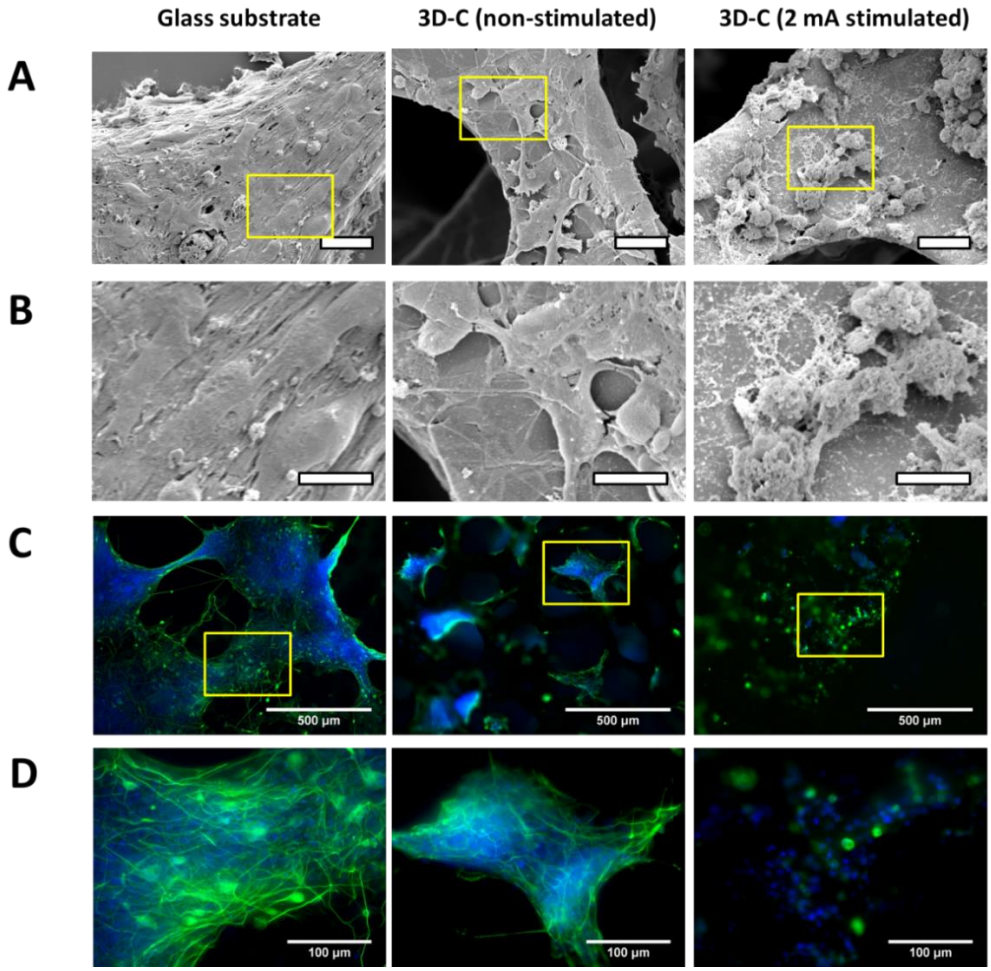

Figure 3*: (A) SEM images and (B-C) Immunofluorescence images of (hNPCs) differentiated after 7 days. From left to right: cells grown on glass substrate, in 3D-C scaffolds without electrical stimulation, and with electrical stimulation of 2 mA over 3 days. The samples were stained with TUJ1 (green channel) and DAPI (blue channel). Figure B and D show the zoomed-in images of the region of interest marked by yellow boxes in figure A and C, respectively. Scale bars are 20 µm,10 µm, 500 µm, and 100 µm in A, B, C, and D, respectively.*

From this, the milli-ampere range was determined to be too intense and the micro-ampere range was focused on instead. Two electrical stimulation durations, 3 days and 7 days, were also assessed to determine how long electrical stimulation should be applied.

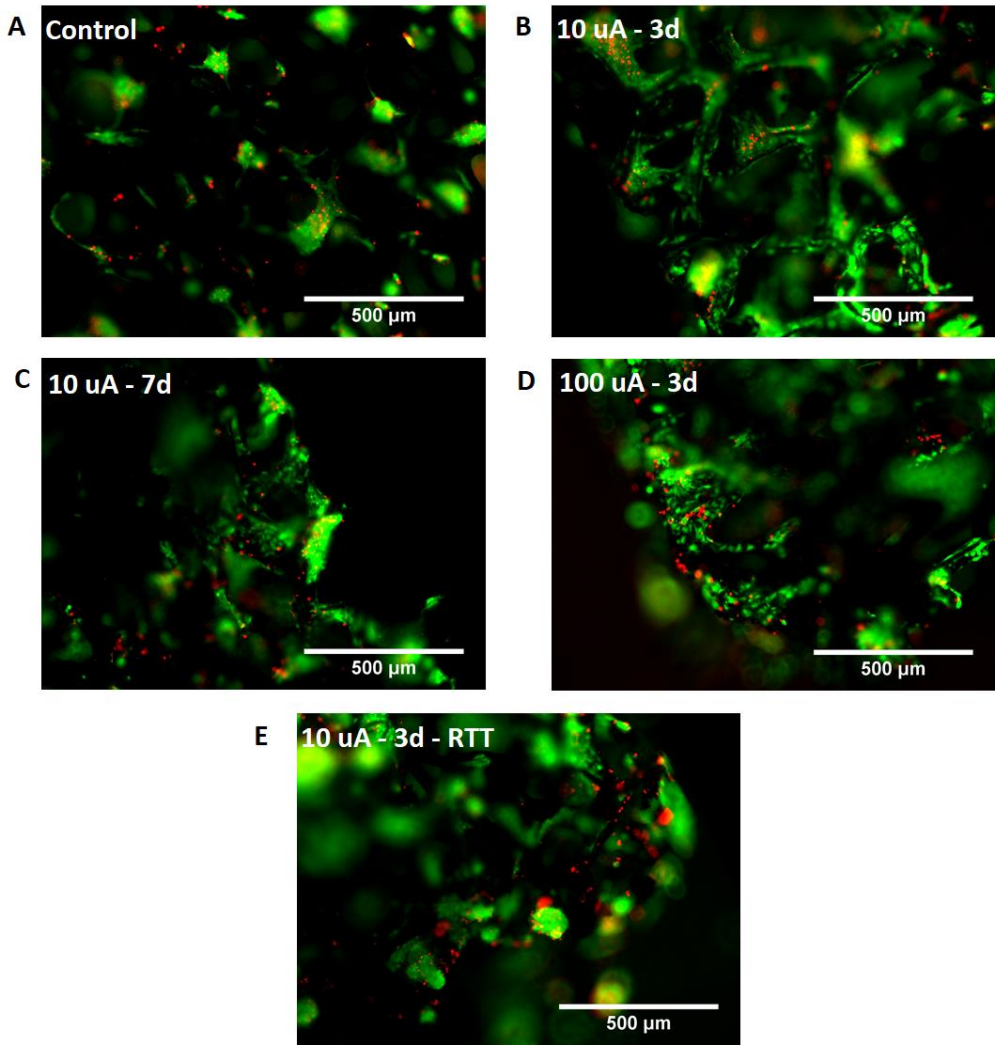

Figure 4*: Live/dead assay seven days after stimulation to optimize stimulation current and treatment time. (A) Unstimulated CTRL cells. (B) CTRL cells stimulated with 10 µA for 3 days. (C) CTRL cells stimulated with 10 µA for 7 days. (D) CTRL cells stimulated with 100 µA for 3 days. (E)RTT cells stimulated with 10 µA for 3 days. Green color denotes the Calcein-AM staining of the live-cell population, while red color denotes the EthD-1 staining of the dead-cell population.*

Qualitative analysis of Calcein-AM and EthD-1 staining assays (live/dead assays) were done to determine if either the micro-current amperage or the chosen electrical stimulation duration reduced cell viability (figure 4). The live/dead assay indicated that both the 10 µA and 100 µA did not have a negative impact on cell viability (figure 4B and 4D). The duration of 3 days or 7 days also did not have a considerable impact on cell viability (figure 4B and 4C). Overall, although dead cells (indicated by red stain of EthD-1) were visible in all the samples, the milli-ampere current range and 3 or 7 day stimulation duration did not affect the cell viability negatively compared to the control. These electrical stimulation parameters were also applied to the RTT cells to ensure they would not be

detrimental to their viability. It was observed that 10 μA for 3 days did not have a negative effect on RTT cell viability (figure 4E).

Because the goal of this study was to optimize neuronal maturation, the protein expression of MAP2 and TUJ1 was analysed to examine how neuronal differentiation was affected by the amperage and electrical stimulation duration. Western Blot analysis was done 7 days and 11 days after electrical stimulation to measure the MAP2 and TUJ1 expression in each group (figures 5A, 5B and S2). The expression of both MAP2 and TUJ1 was lowest in the samples treated with 100 μA. The electrical stimulation treatment of 10 μA over 3 days showed the largest enhancement in MAP2 and TUJ1 expression between day 7 and day 11. The electrical stimulation treatment of 10 μA for 7 days, on the other hand, showed the highest expression of the TUJ1 and MAP2 7 days post-treatment, but the neuronal marker expression was reduced by day 11 post-treatment.

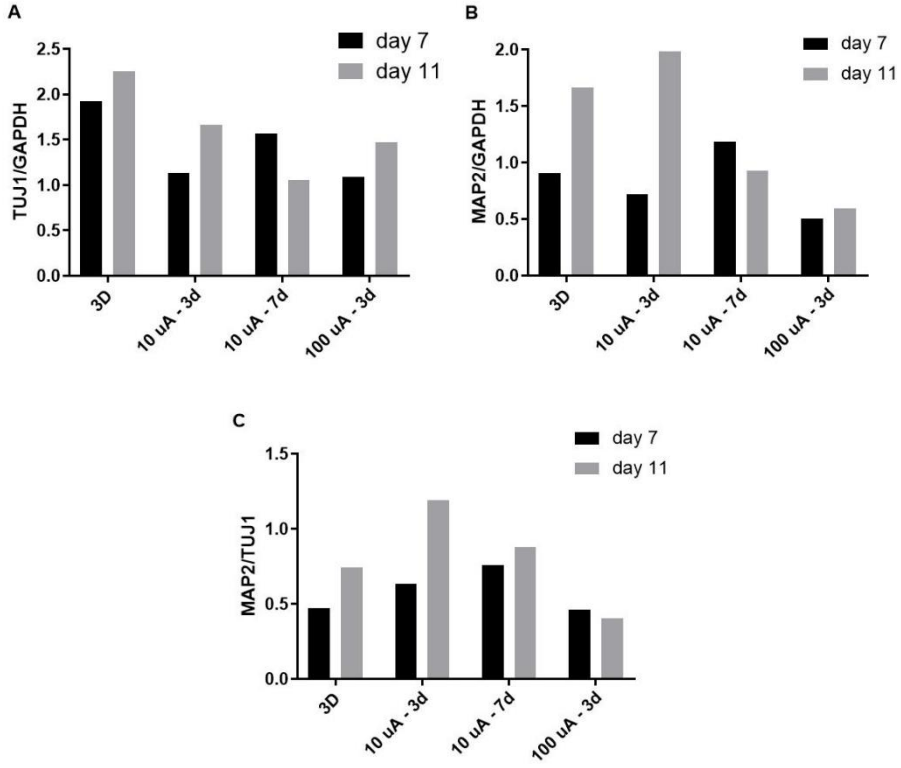

Figure 5*: Western Blot at day 7 and day 11 to determine optimal current and duration for electrical stimulation using CTRL cells. (A) TUJ1 protein expression at day 7 and day 11. (B) TUJ1 protein expression at day 7 and day 11. (C) Ratio of MAP2 and TUJ1 expression. All data represent the average from 3 scaffolds from one batch of cells (3 technical replicas), thus SD was not shown*

The ratio of MAP2/TUJ1 was used as an indicator of neuronal maturation (figure 5C). The cells treated with electrical stimulation with 10 μA over 3 days showed a higher MAP2/TUJ1 expression than the unstimulated samples at day 7 and the highest MAP2/TUJ1 of all the samples at day 11. This suggested that the electrical stimulation parameters of 10 μA for 3 days could be beneficial for neuronal differentiation and maturation. As the goal of this study was to optimize the *in vitro* culture system for neuronal maturation, the parameters of 10 μA over a three-day period were chosen.

Taken together, these optimization data suggest that the 3-day stimulation period with 10 μA was the least detrimental to cell viability, most effective in promoting neuronal maturation, and tolerable for the RTT cells. Therefore, this stimulation parameter was chosen for the following experiments in this study.

3.4. Effect of E-stimulation on the Maturation of CTRL and RTT Cells

It has been reported that the brains of RTT patients, mouse models of RTT, and *in vitro* models of the disorder, showed reduced neuronal maturation compared to their wild-type counter-parts (Kim et al. 2011, Kishi and Macklis 2004, Neul and Zoghbi 2004) . To determine if e-stimulation can improve neuronal differentiation and maturation of RTT NPCs, semi-quantitative analysis of immunofluorescent markers was used to assess development of cells in each treatment group. The immunofluorescent markers, DCX, and MAP2 were used as indicators of the degree of neuronal maturation. The marker DCX was used to identify immature neurons (at the day 7 timepoint) while MAP2 identified mature neurons (at the day 21 timepoint) in this study. The marker TUJ1 was used as a pan-neuronal marker to assess the population of NPCs that committed to neurons. The number of cells positive for the neuronal markers relative to the total number of cells was used to quantify the percentage of neurons of different maturity and the extent to which NPCs differentiated into neurons.

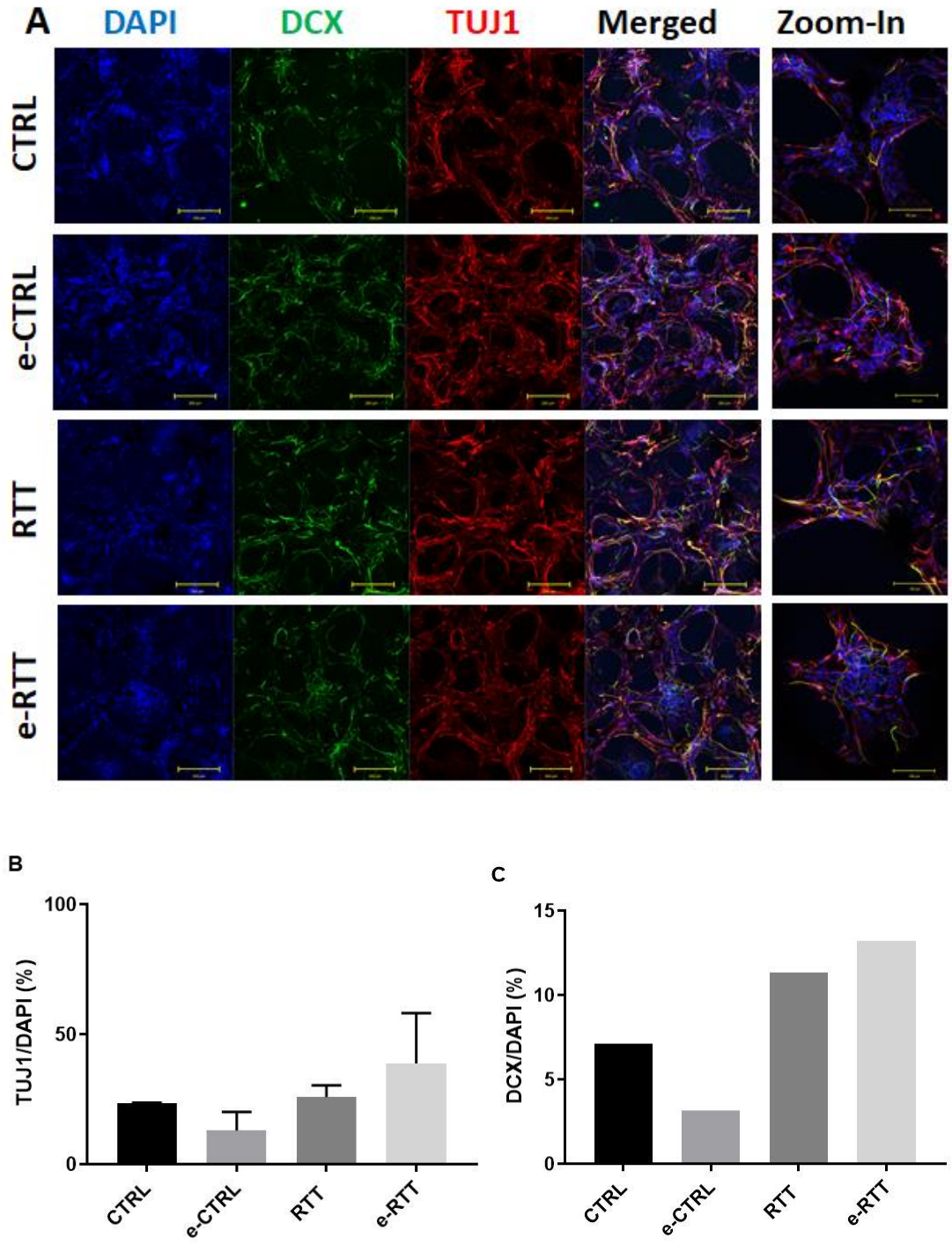

Figure 6*: Imaging and semi-quantitative analysis at the day 7 timepoint. (A) Confocal images of 3D neuronal network (TUJ1/DCX/DAPI) at 10x magnification (scale bar = 200 µm) and zoomed-in at 20x magnification (scale bar = 100 µm). (B) Percentage of cells positive for TUJ1 (C) Percentage cells positive for DCX. Data in (B) is reported as mean +/- SE, n=3 from 2 biological replicas. Data in (C) represent the average from 3 technical replicas, thus SD was not shown*

At the day 7 timepoint, DCX+ and TUJ1+ cells were visible in all treatment groups (figure 6A) indicating neurogenesis had already begun. The e-RTT cells consisted of a higher percentage of

TUJ1+ cells compared to RTT cells (figure 6B), however this difference was not statistically significant. There were fewer TUJ1+ cells in e-CTRL compared to CTRL cells, although these differences were also not statistically significant. The e-RTT cells had a larger percentage of immature neurons (higher percentage of DCX+ cells) as compared to RTT cells. The e-CTRL cells had a lower percentage of DCX+ cells and, by extension, fewer immature neurons compared to the CTRL cells.

The mRNA and protein expression of the TUJ1 and MAP2 at the day 7 timepoint were quantified using RT-qPCR (figures 7A & 7B) and Western Blot, respectively (figures 7C & 7D).

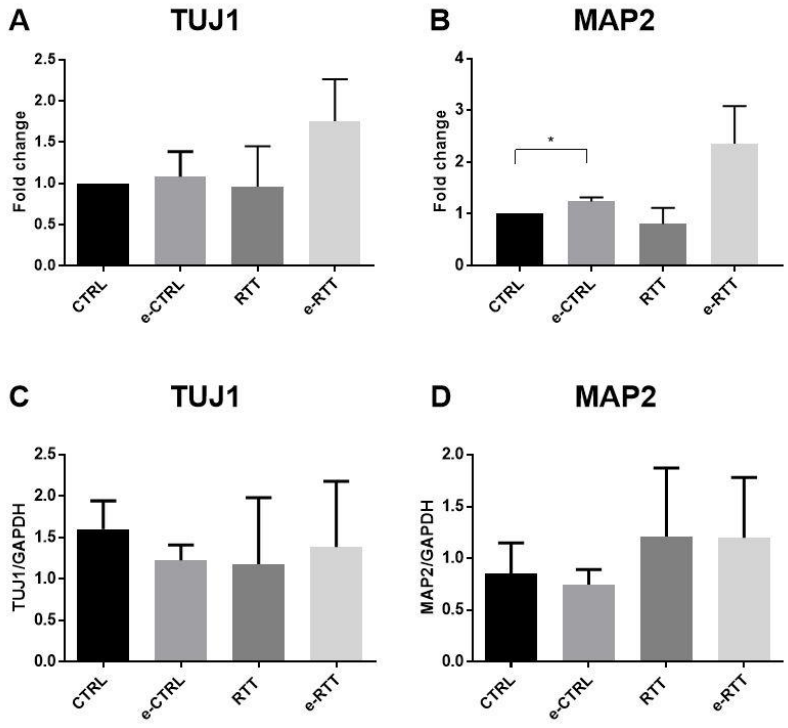

Figure 7: *Quantitative analysis of TUJ1 and MAP2 expression at day 7. (A) qPCR quantification of TUJ1 mRNA expression. (B) qPCR quantification of MAP2 mRNA expression. (C) Western Blot quantification of TUJ1 protein expression. (D) Western Blot quantification of MAP2 protein expression. All data represent mean +/- SE, n =3. Significance criteria was set as p<0.05 (* p<0.05)*

Elevated expression of both genes was seen in all treatment groups at the day 7 timepoint as shown in figures 7A and 7B. Treatment groups that underwent e-stimulation had higher levels of MAP2 than their non-stimulated counterparts. E-stimulation had a mild effect on MAP2 expression in

CTRL cells resulting in expression that was 1.23-fold higher than non-stimulated CTRL cells. However, there was no significant changes in MAP2 protein expression in e-CTRL as compared to CTRL group although MAP2 protein in e-stimulated CTRL cells was slightly lower than that of non-stimulated CTRL cells. E-stimulation had a more considerable impact on RTT cells resulting in a 3.34-fold higher MAP2 mRNA expression than non-stimulated RTT cells. There was no difference in MAP2 protein expression though between e-RTT and RTT cells, as both had a 1.2-fold increase.

Increased TUJ1 mRNA expression in e-stimulated CTRL and RTT samples compared to non-stimulated samples was also noted (1.09-fold and 2.23-fold respectively) but there was no statistical significance. Western blot results also indicated there were no statistically significant differences between TUJ1 protein expression in cells that underwent e-stimulation compared to those that were un-stimulated in either cell type, CTRL or RTT cells. Taken together, it can be concluded that e-stimulation did not have a significant effect on the number of TUJ1+ cells or the expression of TUJ1. On the other hand, e-stimulation led to a trend of increased expression of MAP2 for both groups (though this was not seen at the protein level) and increased the percentage of DCX+ RTT cells at the day 7 timepoint. The suggested enhanced maturation, was further supported by an increase Syn1 expression in the e-stimulated RTT cells compared to non-stimulated RTT cells at day7 and day 11 (figure S3). Expression of Nestin was also assessed. It was found that Nestin expression slightly decreased with e-stimulation for both CTRL and RTT at day 7 and slightly decreased in e-CTRL at day 11, however these differences were not statistically significant (figure S4).

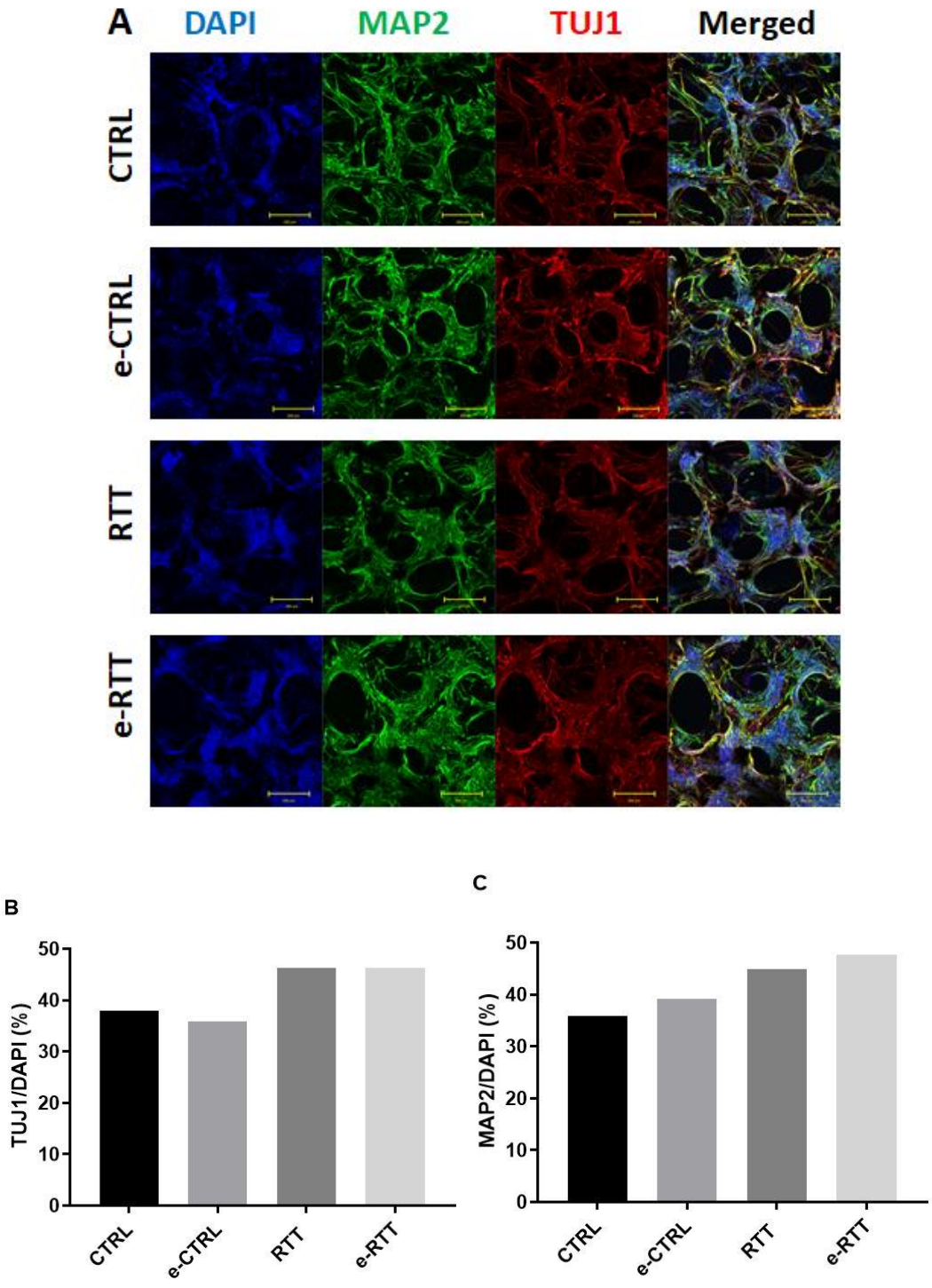

Figure 8: *Imaging and semi-quantitative analysis of cell maturation at the day 21-timepoint. (a) Confocal images of 3D neuronal network (TUJ1/MAP2/DAPI) at 10x magnification. (B) Percentage of cells positive for TUJ1 (C) Percentage cells positive for MAP2. Data in (B) and (C) represent the average from 3 technical replicas, thus SD was not shown*

At day 21, the percentage of TUJ1+ cells in the CTRL, e-CTRL, RTT and e-RTT populations increased considerably compared to day 7 with the largest increase being that of the e-CTRL group

(from 13% at day 7 to 36% at day 21) and the lowest being that of e-RTT group (from 38% at day 7 to 46% at day 21). The percentage of MAP2+ cells increased after electrical stimulation for both CTRL and RTT cells (figure 8c). The percentage of MAP2+ cells was 2.8% higher in e-RTT cells compared to RTT cells. This is a minimal difference and thus at day 21 there was not considered to be any difference between the maturation of e-RTT and RTT cells. The percentage of MAP2+ cells was only 3.2% greater in e-CTRL cells compared to the CTRL cells also suggesting that at day 21 there was no significant difference between the maturation of the cells in the two groups.

Differences in cell morphology between treatment groups was also investigated as it is known that RTT cells typically display morphological defects, including smaller soma size (Cheung et al. 2011, Goh 2017, Marchetto et al. 2010). The abnormally small soma size observed in RTT cells is speculated to be due to dysfunctional osmoregulation, whereby *in vivo* magnetic resonance imaging and spectroscopy of the brains of Mecp2-/y mice showed altered osmolyte profiles (Viola et al. 2007). The small soma size could also be indicative of reduced potential for cellular growth (X. H. Zhang et al. 2006, Baburina and Jackowski 1999). This is congruent with the observation of reduced phosphatidylcholine (an important component of the cellular membrane) turnover in Mecp2-/y mice compared to controls (Viola et al. 2007), and also the altered levels of lipid metabolites in neurons derived from RTT patient-specific iPS cells (Chin et al. 2016).

To determine if e-stimulation could help to increase the average soma size of RTT cells so that they are more similar to CTRL cells, the soma size of e-RTT cells at day 7 and day 21 were analysed. As cells on the 3D scaffold are on different planes, a population of cells from at least 50 planes was considered in this analysis. Similar to the measurement of soma size in histological sections of brain tissue, because all sample groups were seeded on the same type of scaffold and confocal z-stacks images were obtained using the same method, it was assumed that variations in soma size due to projection will be consistent among the different sample groups.

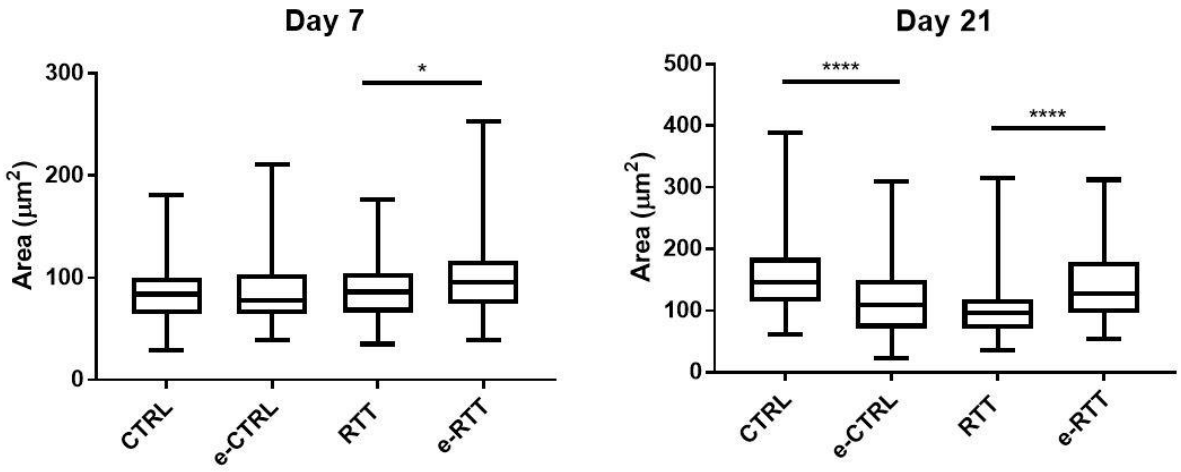

Figure 9: *Median and quartile ranges of soma area of differentiated neuronal progenitor cells. (A) At the day 7 timepoint. (B)At the day 21 timepoint. Data obtained in both (A) and (B) is from 80 cells of each group and one batch of hNPCs. Significance criteria was set as p<0.05. (* p<0.05, **** p<0.0001)*

It was found that e-stimulation of RTT cells resulted in an increase in soma size, compared to non-stimulated RTT cells at both day 7 and day 21 (figure 9). At day 7 the e-RTT cells were 12% larger than the RTT cells. There was no significant difference between the average soma size of CTRL and e-CTRL cells at day 7. The difference between the e-stimulated cells and their non-stimulated counterparts was considerably larger at the day 21 time-point. The e-CTRL cells were significantly smaller than their non-stimulated counterparts; however, the e-RTT cells were significantly larger than the RTT cells. The e-RTT cells were 37% larger than the RTT cells. Overall, e-stimulation increased the average soma size of the RTT cells with significant increases being seen on day 7 and day 21.

4. Discussion

This study outlines the development of a novel approach to analyse the effect of electrical stimulation on patient specific cell lines, specifically iPSC-derived hNPCs, *in vitro* using a 3D graphene scaffold system. Two-dimensional and three-dimensional graphene structures have previously been investigated as scaffold material for neuronal stem cell maturation with positive results. Graphene supports the adhesion, proliferation and differentiation of induced pluri-potent stem cells and neuronal stem cells (Bouzid et al. 2016). It is also known that graphene scaffolds can be

used to electrically stimulate neuronal stem cells (Ding et al. 2015, Park et al. 2011, Shin et al. 2016). Considering that graphene scaffolds can support iPSCs and NPCs and offer a platform for electrical stimulation, we propose the use of these scaffolds as *in vitro* culture-based models of electrically stimulative therapeutic techniques for the central and peripheral nervous system, especially those that are highly invasive such as deep brain stimulation.

Deep brain stimulation has proven to be an effective therapy for movement disorders and has been shown to be promising as a treatment of psychiatric disorders, cognitive disorders, epilepsy and recently, childhood intellectual disability disorders including Rett syndrome (Hao et al. 2015, Li et al. 2013). The effect of electrical stimulation on Rett cells has only been shown in mouse models. In these models, it was found that DBS lead to an increase in hippocampal neurogenesis which can alleviate some of the cognitive disabilities associated with Rett syndrome. Due to the essential neurological differences between mouse models and humans, the results of the mouse modelling may be considered positive but do not necessarily accurately describe the effect that the treatment will have in human neuronal cells. Thus, an *in vitro* model using iPSC-derived NPCs, such as the one reported in this study, can be used to study the effects of electrical stimulation in RTT and supplement *in vivo* models. However, given that RTT is a clinical disorder, the behaviour of the organism still needs to be taken into consideration when examining the efficacy of a potential treatment method. Thus, once any improvement in the RTT phenotype is established in the *in vitro* model, the animal model would still have to be used to aid in conclusively determining the effectiveness of the treatment.

To assess the potential of the graphene scaffold as an *in vitro* model of electrical stimulation, a pilot study on the effects of electrical stimulation on the maturation of human iPSC-derived NPCs from RTT patients was performed. The method of fabrication of the 3D graphene scaffold used in this study resulted in high purity graphene, with high conductivity and negligible amounts of Ni residue. A three-dimensional scaffold was chosen for this study as it has been shown that 3D systems prompt physiological responses more like those *in vivo* than 2D systems (Zhang et al. 2016). Three-dimensional scaffold systems consider the natural 3D microenvironment of cells and better mimic *in*

vivo cell behaviours by introducing physical constraints to cells and influencing spatial organization of cell surface receptors (Edmondson et al. 2014). Close mimicking of *in vivo* conditions is essential as reliable results are necessary to justify *in vivo* testing of therapies and screen potential therapies with correctness thus avoiding waste of resources or, alternatively, overlooking useful therapies.

In this study, iPSCs were derived from patient fibroblasts from a cell bank. As the motivation of the study was to demonstrate the application of the 3D graphene scaffold with the RTT cells as an *in vitro* model for electrical stimulation, the RTT NPCs were derived from one patient only. The iPSC derived NPCs readily adhered to the graphene foam scaffold and formed a neural network by the first week (figure 3A). By the third week they were largely confluent growing both on the surface of the scaffold and within the scaffold (figure 8A). The scaffold was also impervious to the effects of electrical stimulation. No damage to the scaffold was noted after multiple rounds of electrical stimulation with varying currents in both the micro and milli-ampere range. The electrical stimulation parameters in this study were optimized for both the control cells and the RTT cells. The micro-current range used in this study was lower than that used in actual DBS therapy, 3 mA. However, this is because the conductivity of the graphene foam, 58.8 S/m, is considerably higher than the conductivity of white and grey matter in the brain, whose conductivities are in the range of 0.1-1 S/m, thus a lower voltage is required to generate the same potential drop (Kuncel and Grill 2004).

Though the scaffold supports cell proliferation and differentiation there are some potential limitations to using graphene as a tissue engineering material, namely the non-biodegradability and potential *in vivo* toxicity. Graphene can induce cytotoxic effects as it shows oxidative potentials in biological systems and can generate oxidative debris *in vivo* (Gurunathan and Kim 2016, Edmondson et al. 2014, Shin et al. 2016). *In vitro* graphene toxicity is highly dependent on shape and manufacturing method (Zhang et al. 2010). Graphene foams have been demonstrated in both this paper and others to be non-cytotoxic and highly accommodating to cell adhesion. Chemical vapor deposition allows for high purity graphene reducing the potential for cytotoxicity caused by impurities. The nickel template used in chemical vapor deposition poses a potential cytotoxicity risk however, thorough and complete removal can alleviate this risk. Coatings, such as laminin, enhance

cell biocompatibility and further reduce the risk of cytotoxicity. Another potential concern from the regulatory authorities, one that is common in all *in vitro* devices, will be the accuracy of the test. However, for the application of the 3D *in vitro* Rett syndrome model proposed in this paper, the *in vitro* platform will be used as a higher throughput, more economical and more human relevant screening. It is not intended that this system be used as the sole analysis of therapeutic potential. Any product or result derived from the model will have to be further verified with *in vivo* modelling and clinical trials. Thus, for the application of this model, as a basic science research on the understanding of the DBS mechanism, regulatory approval will not be required.

The preliminary results collected in this study show that e-stimulation of RTT cells has a positive impact on their initial maturation. At the day 7 timepoint improvements in the maturation of stimulated RTT cells could be seen in comparison to non-stimulated RTT cells. E-stimulated RTT cells had greater amounts of differentiated cells that were more mature than their non-stimulated counterparts. This was evident as e-RTT cells had higher percentages of DCX+ cells than their non-stimulated counterparts. Analysis with RT-qPCR showed there was considerable increases in the expression of the mature neuronal marker MAP2 in e-RTT cells compared to non-stimulated RTT cells. Morphology of developing RTT cells also seemed to be improved as e-stimulated Rett cells had larger average soma than their non-stimulated counterparts after 7 days. The mechanism by which electrical stimulation improved maturation and soma size is out of the scope of this paper but would be interesting to investigate in future studies. While most of the differences between stimulated and non-stimulated RTT cells was mild, the increased MAP2 expression and the increased soma size of e-stimulated RTT and the differencing responses to e-stimulation from CTRL and RTT cells implies that an enhancement in RTT neuronal maturation could be a potential reason for the improvement in patients who undergo DBS.

There are currently few to no papers describing methods of translating culture-based *in vitro* DBS analysis to *in vivo* DBS analysis. To the best of the authors' knowledge, of the papers that could be found, most focused on predicting the change of DBS electrode impendence over time. Though these *in vitro* analyses of electrode impedance employ aqueous solutions and are not culture based,

the methods used to translate *in vitro* and *in vivo* results in these studies do provide some useful advice for potentially translating cell-culture based *in vitro* analysis to *in vivo* analysis. A commonly used method is the use of an equivalent circuit (Badstubner et al. 2013, Wei and Grill 2009, Lempka et al. 2009). This method can be employed to study the electrochemistry at the electrode-tissue interface *in vivo* and compare it to that *in vitro*. To study the effects on cell morphology, histoimmunochemical analysis and electron-microscopy of tissue samples collected after *in vivo* treatment can be analysed (Badstubner et al. 2013, Anderson et al. 2004). In these studies, analysis was done to determine how cells changed at the electrode-tissue interface, but in the case of complementary culture-based *in vitro* analysis, these tests could be used to compare *in vivo* cell morphology changes with those seen *in vitro.* Pending further studies on the similarity between the response of cells in this study's proposed system and the response to DBS seen in brain slices, it can be extrapolated that data gleaned from the proposed *in vitro* system can be used to model the situation *in vivo*. This lack of an available *in vitro-in vivo* translation model highlights the needs to develop *in vitro* models and methods.

The similarity in the percentage of mature cells between RTT and e-RTT populations and at day 21 indicated that the positive effects of the e-stimulation offered an initial advantage to e-RTT cells but the benefits reduced with time. Loss of benefit after abruptly stopping DBS therapy, also known as washout time, has been observed in the use of DBS as a therapy for Parkinson's disease. It was observed that when DBS treatment was abruptly stopped symptoms that were eliminated by the treatment quickly returned (Cooper et al. 2013). This suggests that future studies should increase the frequency with which electrical stimulation is applied throughout the maturation of NPCs to see if it can offer better long-term effects on maturation and see whether expression of more mature markers, such as NeuN or GABA, are affected. Future use and development of this system could also help to determine the underlying mechanism of electrical stimulation and the benefit of electrical stimulation on neurogenesis and neuronal integration. This might also explain the initial improvement and the proceeding reduction in benefit at the day 21 timepoint.

5. Conclusions

The three-dimensional graphene scaffold culture system used in this study can be successfully used to study the effects of electrical stimulation of both wild-type and RTT syndrome iPSC-derived hNPCs. The scaffold can support the adherence, differentiation and maturation of patient specific iPSC-derived hNPCs and can be used to deliver three-dimensional electrical stimulation. This system has also been shown to be a novel *in vitro* model of the effects of electrical stimulation on the maturation of RTT neural progenitor cells and it could be used in conjunction with *in vivo* mouse models to assess the candidacy of deep brain stimulation as a therapy for Rett syndrome patients. The experimental evidence collected using this system suggests that electrical stimulation has a mild, but promising, effect on the maturation of RTT NPCs indicating that further *in vitro* analysis using this system should be pursued.

6. References

Albertsson, A.C. & Varma, I.K. 2003, "Recent developments in ring opening polymerization of lactones for biomedical applications.", *Biomacromolecules*, vol. 4, no. 6, pp. 1466-1486.

Ameri, S.K., Singh, P.K., D'Angelo, R., Stoppel, W., Black, L. & Sonkusale, S.R. 2016, "Three dimensional graphene scaffold for cardiac tissue engineering and in-situ electrical recording", , pp. 4201.

Amir, R.E., Van den Veyver, I.B., Schultz, R., Malicki, D.M., Tran, C.Q., Dahle, E.J., Philippi, A., Timar, L., Percy, A.K., Motil, K.J., Lichtarge, O., Smith, E.O., Glaze, D.G. & Zoghbi, H.Y. 2000, "Influence of mutation type and X chromosome inactivation on Rett syndrome phenotypes", *Annals of Neurology*, vol. 47, no. 5, pp. 670-679.

Amir, R.E., Van den Veyver, I.B., Wan, M., Tran, C.Q., Francke, U. & Zoghbi, H.Y. 1999, "Rett syndrome is caused by mutations in X-linked MECP2, encoding methyl-CpG-binding protein 2", *Nature genetics*, vol. 23, no. 2, pp. 185-188.

Ananiev, G., Williams, E.C., Li, H. & Chang, Q. 2011, "Isogenic pairs of wild type and mutant induced pluripotent stem cell (iPSC) lines from Rett syndrome patients as in vitro disease model", *PLoS One*, vol. 6, no. 9, pp. e25255.

Anderson, T., Hu, B., Pittman, Q. & Kiss, Z.H.T. 2004, "Mechanisms of deep brain stimulation: an intracellular study in rat thalamus", *The Journal of physiology*, vol. 559, pp. 301-313.

Asaka, Y., Jugloff, D.G., Zhang, L., Eubanks, J.H. & Fitzsimonds, R.M. 2006, "Hippocampal synaptic plasticity is impaired in the Mecp2-null mouse model of Rett syndrome", *Neurobiology of disease*, vol. 21, no. 1, pp. 217-227.

Baburina, I. & Jackowski, S. 1999, "Cellular responses to excess phospholipid", *The Journal of biological chemistry*, vol. 274, no. 14, pp. 9400-9408.

Badstubner, K., Kroger, T., Mix, E., Gimsa, U., Benecke, R. & Gimsa, J. 2013, "Electrical Impedance Properties of Deep Brain Stimulation Electrodes during Long-Term In-Vivo Stimulation in the Parkinson Model of the Rat" in *Biomedical Engineering Systems and Technologies: 5th International Joint Conference, BIOSTEC 2012, Vilamoura, Portugal, February 1-4, 2012, Revised Selected Papers*, eds. J. Gabriel, J. Schier, S. Van Huffel, et al, Springer Berlin Heidelberg, Berlin, Heidelberg, pp. 287-297.

Belichenko, P.V., Oldfors, A., Hagberg, B. & Dahlstrom, A. 1994, "Rett syndrome: 3-D confocal microscopy of cortical pyramidal dendrites and afferents", *Neuroreport*, vol. 5, no. 12, pp. 1509-1513.

Bienvenu, T., Carrie, A., de Roux, N., Vinet, M.C., Jonveaux, P., Couvert, P., Villard, L., Arzimanoglou, A., Beldjord, C., Fontes, M., Tardieu, M. & Chelly, J. 2000, "MECP2 mutations account for most cases of typical forms of Rett syndrome", *Human molecular genetics,* vol. 9, no. 9, pp. 1377-1384.

Bosi, S., Rauti, R., Laishram, J., Turcho, A., Lonardoni, D., Nieus, T., Prato, M., Scaini, D. & Ballerini, L. 2015, "From 2D to 3D: novel nanostructured scaffolds to investigate signalling in reconstructed neuronal networks", *Scientific Reports,* vol. 5, no. 1, pp. 9562.

Bouzid, T., Sinitskii, A. & Lim, J.Y. 2016, "Graphene platform for neural regenerative medicine", *Neural Regeneration Research,* vol. 11, no. 6, pp. 894-895.

Casanova, M.F., Buxhoeveden, D., Switala, A. & Roy, E. 2003, "Rett syndrome as a minicolumnopathy", *Clinical neuropathology,* vol. 22, no. 4, pp. 163-168.

Chahrour, M. & Zoghbi, H.Y. 2007, "The story of Rett syndrome: from clinic to neurobiology", *Neuron,* vol. 56, no. 3, pp. 422-437.

Chao, H.T., Zoghbi, H.Y. & Rosenmund, C. 2007, "MeCP2 controls excitatory synaptic strength by regulating glutamatergic synapse number", *Neuron,* vol. 56, no. 1, pp. 58-65.

Cheung, A.Y., Horvath, L.M., Grafodatskaya, D., Weksberg, R., Hotta, A., Carrel, L. & Ellis, J. 2011, "Isolation of MECP2-null Rett Syndrome patient hiPS cells and isogenic controls through X-chromosome inactivation.", *Human Molecular Genetics,* vol. 20, no. 11, pp. 2103-2115.

Chin, E.W.M., Marcy, G., Yoon, S., Ma, D., Rosales, F.J., Augustine, G.J. & Goh, E.L.K. 2016, "Choline Ameliorates Disease Phenotypes in Human iPSC Models of Rett Syndrome", *NeuroMolecular Medicine,* vol. 18, no. 3, pp. 364-377.

Cooper, S.E., McIntyre, C.C., Fernandez, H.H. & Vitek, J.L. 2013, "Association of Deep Brain Stimulation Washout Effects With Parkinson Disease Duration", *JAMA Neurology,* vol. 70, no. 1, pp. 95-99.

Ding, X., Liu, H. & Fan, Y. 2015, "Graphene-Based Materials in Regenerative Medicine", *Advanced Healthcare Materials,* vol. 4, pp. 1451-1468.

Dreyer, D.R., Park, S., Bielawski, C.W. & Ruoff, R.S. 2010, "The chemistry of graphene oxide", *Chemical Society Reviews,* vol. 39, no. 1, pp. 228-240.

Edmondson, R., Broglie, J.J., Adcock, A.F. & Yang, L. 2014, "Three-Dimensional Cell Culture Systems and Their Applications in Drug Discovery and Cell-Based Biosensors", *Assay and Drug Development Technologies,* vol. 12, no. 4, pp. 207-218.

Gilje, S., Han, S., Wang, M., Wang, K.L. & Kaner, R.B. 2007, "A Chemical Route to Graphene for Device Applications", *Nano Letters,* vol. 7, no. 11, pp. 3394-3398.

Goh, E. 2017, "Rett syndrome: a sex-biased neuro developmental disorder", *The Biochemist,* vol. 39, pp. 30-33.

Gurunathan, S. & Kim, J. 2016, "Synthesis, toxicity, biocompatibility, and biomedical applications of graphene and graphene-related materials", *International Journal of Nanomedicine,* vol. 11, pp. 1927-1945.

Hao, S., Tang, B., Wu, Z., Ure, K., Sun, Y., Tai, H., Gao, Y., Patel, A., Curry, D.J., Samaco, R.C., Zoghbi, H.Y. & Tang, J. 2015, "Forniceal deep brain stimulation rescues hippocampal memory in Rett syndrome mice", *Nature,* vol. 526, no. 7573, pp. 430-434.

Huppke, P., Laccone, F., KrÃ¤mer, N., Engel, W. & Hanefeld, F. 2000, "Rett syndrome: analysis of MECP2 and clinical characterization of 31 patients", *Human molecular genetics,* vol. 9, no. 9, pp. 1369-1375.

Kim, K.Y., Hysolli, E. & Park, I.H. 2011, "Neuronal maturation defect in induced pluripotent stem cells from patients with Rett syndrome", *Proceedings of the National Academy of Sciences,* vol. 108, no. 34, pp. 14169-14174.

Kishi, N. & Macklis, J.D. 2004, "MECP2 is progressively expressed in post-migratory neurons and is involved in neuronal maturation rather than cell fate decisions", *Molecular and Cellular Neuroscience,* vol. 27, no. 3, pp. 306-321.

Kocabicak, E., Temel, Y., Hollig, A., Falkenburger, B. & Tan, S.K.H. 2015, "Current perspectives on deep brain stimulation for severe neurological and psychiatric disorders", *Neuropsychiatric Disease and Treatment,* vol. 11, pp. 1051-1066.

Kozera, B. & Rapacz, M. 2013, "Reference genes in real-time PCR", *Journal of Applied Genetics,* vol. 54, no. 4, pp. 391-406.

Kuncel, A.M. & Grill, W.M. 2004, "Selection of stimulus parameters for deep brain stimulation", *Clinical Neurophysiology,* vol. 115, no. 11, pp. 2431-2441.

Lee, S.S., Wan, M. & Francke, U. 2001, "Spectrum of MECP2 mutations in Rett syndrome", *Brain & development,* vol. 23 Suppl 1, pp. S138-43.

Lempka, S.F., Miocinovic, S., Johnson, M.D., Vitek, J.L. & McIntyre, C.C. 2009, "In vivo impedance spectroscopy of deep brain stimulation electrodes", *Journal of neural engineering,* vol. 6, no. 4, pp. 046001-046001.

Li, N., Zhang, Q., Gao, S., Song, Q., Huan, R., Wang, L., Liu, L., Dai, J., Tang, M. & Cheng, G. 2013, "Three-dimensional graphene foam as a biocompatible and conductive scaffold for neural stem cells", *Scientific Reports,* vol. 3, no. 1, pp. 1604.

Loeblein, M., Perry, G., Tsang, S.H., Xiao, W., Collard, D., Coquet, P., Sakai, Y. & Teo, E.H.T. 2016, "Three-Dimensional Graphene: A Biocompatible and Biodegradable Scaffold with Enhanced Oxygenation", *Advanced Healthcare Materials,* vol. 5, no. 10, pp. 1177-1191.

Lu, H., Ash, R.T., He, L., Kee, S.E., Wang, W., Yu, D., Hao, S., Meng, X., Ure, K., Ito-Ishida, A., Tang, B., Sun, Y., Ji, D., Tang, J., Arenkiel, B.R., Smirnakis, S.M. & Zoghbi, H.Y. 2016, "Loss and Gain of MeCP2 Cause Similar Hippocampal Circuit Dysfunction that Is Rescued by Deep Brain Stimulation in a Rett Syndrome Mouse Model", *Cell Press,* vol. 91, pp. 739-747.

Marchetto, M.C.N., Carromeu, C., Acab, A., Yu, D., Yeo, G.W., Mu, Y., Chen, G., Gage, F.H. & Muotri, A.R. 2010, "A Model for Neural Development and Treatment of Rett Syndrome Using Human Induced Pluripotent Stem Cells", *Cell Press,* vol. 143, pp. 527-539.

Nardone, R., Holler, Y., Tezzon, F., Christova, M., Schwenker, K., Golaszewski, S., Trinka, E. & Brigo, F. 2015, "Neurostimulation in Alzheimer's disease: from basic research to clinical applications", *Neurological sciences : official journal of the Italian Neurological Society and of the Italian Society of Clinical Neurophysiology,* vol. 36, no. 5, pp. 689-700.

Neul, J.L. & Zoghbi, H.Y. 2004, "Rett Syndrome: A Prototypical Neurodevelopmental Disorder", *The Neuroscientist,* vol. 10, no. 2, pp. 118-128.

Park, S.Y., Park, J., Sim, S.H., Sung, M.G., Kim, K.S., Hong, B.H. & Hong, S. 2011, "Enhanced Differentiation of Human Neural Stem Cells into Neurons on Graphene", *Advanced Healthcare Materials,* vol. 23, pp. H263-H267.

Shin, S.R., Li, Y.C., Jang, H.L., Khoshakhlagh, P., Akbari, M., Nasajpour, A., Zhang, Y.S. & Khademhosseini, A. 2016, "Graphene-based materials for tissue engineering", *Advanced Drug Delivery Reviews,* vol. 105, pp. 255-274

Soman, P., Tobe, B.T.D., Lee, J.W., Winquist, A.M., Singec, I., Vecchio, K.S., Snyder, E.Y. & Chen, S. 2013, "Three-dimensional scaffolding to investigate neuronal derivatives of human embryonic stem cells", *Biomedical Microdevices,* vol. 14, no. 5, pp. 829-838.

Thompson, D.M., Koppes, A.N., Hardy, J.G. & Schmidt, C.E. 2014, "Electrical Stimuli in the Central Nervous System Microenvironment", *Annual Review of Biomedical Engineering,* vol. 16, pp. 397-430.

Van der Pauw, L.J. 1958, "A Method of Measuring Specific Resistivity and HALL Effect of Discs of Arbitrary Shape", *Philips Research Reports,* vol. 13, no. 1, pp. 1-9.

Viola, A., Saywell, V., Villard, L., Cozzone, P.J. & Lutz, N.W. 2007, "Metabolic fingerprints of altered brain growth, osmoregulation and neurotransmission in a Rett syndrome model", *PloS one,* vol. 2, no. 1, pp. e157.

Wan, M., Lee, S.S., Zhang, X., Houwink-Manville, I., Song, H.R., Amir, R.E., Budden, S., Naidu, S., Pereira, J.L., Lo, I.F., Zoghbi, H.Y., Schanen, N.C. & Francke, U. 1999, "Rett syndrome and beyond: recurrent spontaneous and familial MECP2 mutations at CpG hotspots", *American Journal of Human Genetics,* vol. 65, no. 6, pp. 1520-1529.

Wei, X.F. & Grill, W.M. 2009, "Impedance characteristics of deep brain stimulation electrodes in vitro and in vivo", *Journal of neural engineering,* vol. 6, no. 4, pp. 046008-046008.

Yavari, F., Chen, Z., Thomas, A.V., Ren, W., Cheng, H.M. & Koratkar, N. 2011, "High sensitivity gas detection using a macroscopic three-dimensional graphene foam network", *Scientific Reports,* vol. 1, pp. 166.

Zhang, X.H., Zhao, C., Seleznev, K., Song, K., Manfredi, J.J. & Ma, Z.A. 2006, "Disruption of G1-phase phospholipid turnover by inhibition of Ca2+-independent phospholipase A2 induces a p53-dependent cell-cycle arrest in G1 phase", *Journal of cell science,* vol. 119, no. Pt 6, pp. 1005-1015.

Zhang, Y., Ali, S.F., Dervishi, E., Xu, Y., Li, Z., Casciano, D. & Biris, A.S. 2010, "Cytotoxicity effects of graphene and single-wall carbon nanotubes in neural phaeochromocytoma-derived PC12 cells", *ACS nano,* vol. 4, no. 6, pp. 3181-3186.

Zhang, Z.N., Freitas, B.C., Qian, H., Lux, J., Acab, A., Trujillo, C.A., Herai, R.H., Nguyen Huu, V.A., Wen, J.H., Joshi-Barr, S., Karpiak, J.V., Engler, A.J., Fu, X.D., Muotri, A.R. & Almutairi, A. 2016, "Layered hydrogels accelerate iPSC-derived neuronal maturation and reveal migration defects caused by MeCP2 dysfunction", *Proceedings of the National Academy of Sciences of the United States of America,* vol. 113, no. 12, pp. 3185-3190.

Zhu, Y., Murali, S., Cai, W., Li, X., Suk, J.W., Potts, J.R. & Ruoff, R.S. 2010, "Graphene and Graphene Oxide: Synthesis, Properties, and Applications", *Advanced Materials,* vol. 22, no. 35, pp. 3906-3924.

Acknowledgements

This research work was partially funded by: National Research Foundation, Prime Minister's Office, Singapore under its Competitive Research Programme (NRF-CRP002-082), under the Research Center of Excellence programme administered by the Mechanobiology Institute of Singapore, the National Medical Research Council (NMRC) - Collaborative Research Programme Grant (CBRG) - (NMRC/CBRG/0094/2015), and the Natural Sciences and Engineering Research Council of Canada Discovery Grant (NSERC 2016040).The authors thank Dr. Muhammad Rizwan for assistance in editing the manuscript and providing helpful comments, and Lidia Luna Puerta for RT-qPCR experiments and data analysis. SM was supported by Natural Science and Engineering Research Council (NSERC) of Canada through the Undergraduate Student Research Awards.